
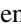
















Observation of a candidate for the $M1$ scissors resonance in odd-odd ^{166}Ho

F. Pogliano ^{1,*} F. L. Bello Garrote ¹ A. C. Larsen ^{1,†} H. C. Berg ^{2,3,4} D. Gjestvang ¹ A. Gørgen ¹
M. Guttormsen ¹ V. W. Ingeberg ¹ T. W. Johansen ¹ K. L. Malatji ^{5,6} E. F. Matthews ⁷ M. Markova ¹ J. E. Midtbø ¹
V. Modamio ¹ L. G. Pedersen ¹ E. Sahin ¹ S. Siem ¹ T. G. Tornyi ^{1,8} and A. S. Voyles ⁷

¹*Department of Physics, University of Oslo, N-0316 Oslo, Norway*

²*Physics Department, Michigan State University, East Lansing, Michigan 48824, USA*

³*National Superconducting Cyclotron Laboratory, Michigan State University, East Lansing, Michigan 48824, USA*

⁴*Joint Institute for Nuclear Astrophysics Center for the Evolution of the Elements,
University of Notre Dame, Notre Dame, Indiana 46556, USA*

⁵*SSC Laboratory, iThemba LABS, P.O. Box 722, Somerset West 7129, South Africa*

⁶*Physics Department, Stellenbosch University, Matieland 7602, South Africa*

⁷*Department of Nuclear Engineering, University of California, Berkeley, California 94720, USA*

⁸*Institute for Nuclear Research (Atomki), 4026 Debrecen, Hungary*



(Received 29 September 2022; accepted 16 February 2023; published 8 March 2023)

The γ -strength function and the nuclear level density for the odd-odd, rare-earth nucleus ^{166}Ho have been extracted from $^{163}\text{Dy}(\alpha, p\gamma)^{166}\text{Ho}$ data using the Oslo method. A structure at ≈ 3 MeV in the γ -strength function is interpreted as the $M1$ scissors resonance. By employing three different methods we find that its strength depends rather strongly on the modeling of the $E1$ strength, while its centroid does not. The ^{166}Ho scissors resonance parameters are consistent with previous results on other rare-earth nuclei.

DOI: [10.1103/PhysRevC.107.034605](https://doi.org/10.1103/PhysRevC.107.034605)

I. INTRODUCTION

Our understanding of the response of rare-earth elements to electromagnetic radiation is far from complete. This region of the nuclear chart is interesting because of the variety in deformation (from close-to-spherical to well-deformed prolate shapes [1]), and it is an ideal region for studying nuclear statistical properties (see, e.g., Refs. [2–6]).

The *scissors resonance* (SR), also called the scissors mode, has received much attention over the years. The SR was originally predicted to be originating from neutrons and protons oscillating against each other like scissor blades in deformed, rotational nuclei [7], but is now understood as a coherent contribution from single-particle couplings between orbitals of the same angular momentum ℓ and j centered at around $E_\gamma = 3$ MeV [8]. While the SR has been observed in many even-even and odd-even nuclei (see, e.g., Refs. [6,8]), it has not yet been studied thoroughly in odd-odd ones, with the notable exception of the two-step cascade experiment on ^{160}Tb by Kroll *et al.* [9].

While many studies have been carried out using the nuclear resonance fluorescence (NRF) technique (see Ref. [8] and references within), this technique has usually been applied in the low excitation-energy region. Counting individual states and transitions becomes increasingly difficult when the density of energy levels increases. To account for the apparent

missing strength in odd- A nuclei, Huxel *et al.* [10] applied a statistical analysis in the case of ^{165}Ho and ^{169}Tm . With such an approach, they were able to obtain an integrated upwards $B(M1) \uparrow$ strength of $\approx 3 \mu_N^2$, in good agreement with previous NRF results on well-deformed even-even nuclei in the rare-earth region [11,12]. Also, Nord *et al.* [13] performed experiments with even better resolution on the same nuclei and thus an improved sensitivity for several odd- A rare-earth nuclei. When the number of energy levels per excitation energy bin $\rho(E_x)$ (or nuclear level density, NLD) becomes larger than ~ 50 – 100 levels per MeV, it is often more useful to consider the statistical properties of the nucleus instead of singular levels and decays. The nuclear excitation energy region between E_x for which $\rho(E_x) > 50 \text{ MeV}^{-1}$ and where particles are still bound is called the quasicontinuum, and two useful quantities here are the NLD and γ -strength function $f(E_\gamma)$, or GSF. The GSF is the statistical counterpart of transition probabilities for the discrete region; it gives us information on which γ energies the nucleus prefers to decay with, and thus an insight into its internal structure and collective modes. A puzzle that is still not fully solved is the seemingly conflicting results on the integrated strength of the SR obtained from different types of experiments. As already mentioned, NRF experiments have revealed a total strength of $\approx 3 \mu_N^2$ for well-deformed rare-earth nuclei. In contrast, experiments utilizing the two-step cascade method following neutron capture [14–16] have found about twice the integrated strength, which is also the case for data analyzed with the Oslo method [3,4,6,17–22]. One possible explanation for this discrepancy is related to the different moments of inertia the

*francesco.pogliano@fys.uio.no

†a.c.larsen@fys.uio.no

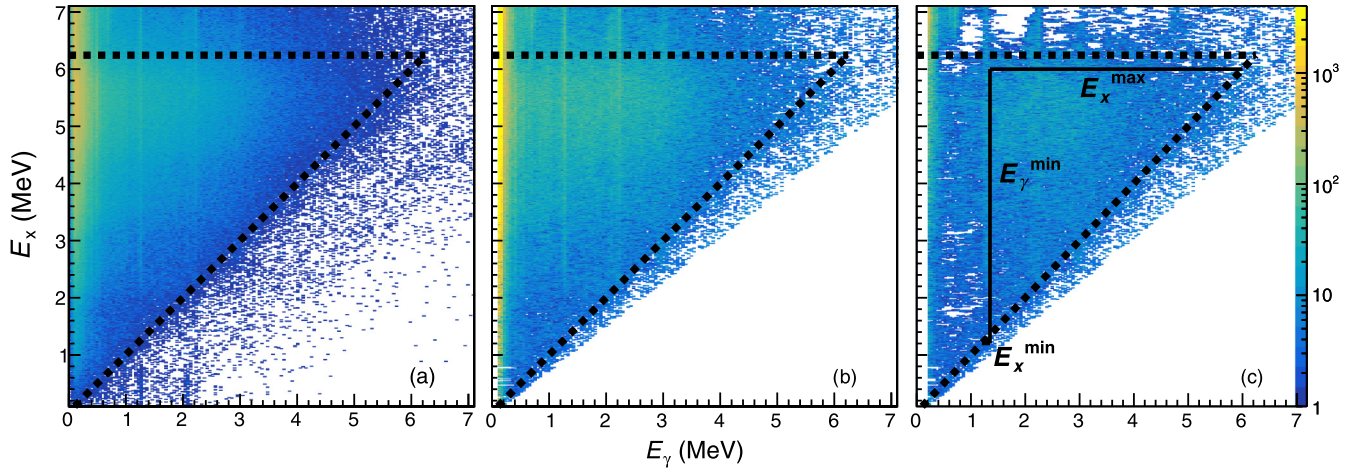


FIG. 1. The (a) raw, (b) unfolded, and (c) first-generation matrices used in the Oslo method analysis. The x axis indicates the γ -ray energy E_γ , while the y axis indicates the excitation energy E_x . The stippled lines indicate the $E_x = E_\gamma$ diagonal and the neutron-separation energy $S_n = 6.244$ MeV.

nucleus attains for ground-state excitations and quasicontinuum decay (for which in the latter case, many quasiparticles are involved; see, e.g., Uhrenholt *et al.* [23]). If this is the case, it would mean that the Brink-Axel hypothesis [24,25] is not valid for the SR; i.e., its properties in the ground state are not the same as those for excited levels. However, as discussed in Ref. [6], there are many possible sources of uncertainties when extracting the integrated SR strength, and they are perhaps so significant that one should be careful making strong conclusions as of now.

This work aims to further investigate the SR in rare-earth, odd-odd nuclei through the data from the $^{163}\text{Dy}(\alpha, p\gamma)^{166}\text{Ho}$ experiment performed at the Oslo Cyclotron Laboratory (OCL). Using the Oslo method, it is possible to simultaneously extract the NLD and the GSF from particle- γ coincidences in charged reaction experiments. In this article, the experimental setup and data analysis are described in Secs. II and III, discussion on implications for scissors mode is given in Sec. IV and a summary is given in Sec. V.

II. EXPERIMENTAL METHOD

The experiment was carried out at the OCL in April 2018 for a period of 6 days, where an α beam of 26 MeV and ≈ 3 -nA intensity was impinged on a ^{163}Dy self-supporting target of 2 mg/cm² thickness and 98.5% enrichment. The Oslo Scintillator Array (OSCAR) and the silicon ring (SiRi) detector arrays were used in order to detect the particle- γ coincidences from the $(\alpha, p\gamma)$ reaction. The γ rays were detected by placing the targets inside OSCAR [26], an array of 30 cylindrical (3.5'' \times 8.5'') LaBr₃(Ce) scintillator detectors mounted on a truncated icosahedron frame, where 28 were operational at the time of the experiment. OSCAR has an energy resolution of 2.7% at $E_\gamma = 662$ keV and a typical time resolution of the prompt timing peak of ≈ 1 –5 ns. Particles were detected using SiRi [27], a ΔE - E particle telescope consisting of a ring of 8 silicon-telescope modules covering 126°–140° in backwards angles (corresponding to 6% of 4π).

Each of these modules consists of a thick (1550 μm) E back detector, and a thin (130 μm) ΔE strip detector segmented in 8 parts in the front covering about 2° each, together forming a system of 64 detectors. Using the ΔE - E technique, we collect particle energy and timing information and represent the event by plotting the deposited energy in the back detector versus the deposited energy in the front strip. This was used in order to separate the various reaction channels and select only the (α, p) data. Given the projectile and ejectile energies, together with the known Q values of the reaction, we are able to calculate the excitation energy of the residual nucleus using the reaction kinematics. With this, an excitation energy vs γ -ray energy matrix called the *raw* coincidence matrix is obtained [see Fig. 1(a)]. From the raw coincidence matrix, the primary γ -ray spectra for each excitation energy can be obtained using the established methodology of the Oslo method [28–30]. This is done by first deconvoluting [28] the raw matrix using the response function of Refs. [26,31] [see Fig. 1(b)] and then extracting the first-emitted γ rays in the decay cascades through a subtraction technique (Fig. 1(c), see Ref. [29]).

Assuming the validity of the generalized Brink-Axel hypothesis [24,25], stating that the GSF is independent of initial and final excitation energy, spin, and parity, we can extract the NLD and GSF from the *primary* γ -ray matrix, also known as the *first-generation* γ -ray matrix. The Brink-Axel hypothesis has been tested for neighboring nuclei of dysprosium [6,32] and is therefore expected to be applicable in this mass region. Fermi's Golden rule [33,34] allows us to apply the ansatz [30]

$$P(E_\gamma, E_x) \propto \mathcal{T}(E_\gamma)\rho(E_x - E_\gamma), \quad (1)$$

where P is the probability for the excited nucleus to decay from excitation energy E_x by emitting a γ ray with energy E_γ , $\rho(E_x - E_\gamma)$ is the level density in the final energy level, and $\mathcal{T}(E_\gamma)$ is the γ -transmission coefficient, from which one can derive the GSF, denoted by f^{XL} , through the relation

$$\mathcal{T}^{XL}(E_\gamma) = 2\pi E_\gamma^{2L+1} f^{XL}(E_\gamma), \quad (2)$$

for γ transitions of electromagnetic character X , multipolarity L , and γ energy E_γ . The GSF is defined as [35]

$$f^{XL}(E_x, E_\gamma, J, \pi) = \frac{\langle \Gamma_\gamma^{XL}(E_x, E_\gamma, J, \pi) \rangle}{D(E_x, E_\gamma, J, \pi) E_\gamma^{2L+1}}, \quad (3)$$

where $\langle \Gamma_\gamma^{XL} \rangle$ is the average partial γ -decay width and D is the mean level spacing. The average partial γ -decay width is also directly connected to the transmission coefficient by [36]

$$\langle \Gamma_\gamma^{XL}(E_x, E_\gamma, J, \pi) \rangle = \mathcal{T}^{XL}(E_x, E_\gamma, J, \pi) \frac{D(E_x, E_\gamma, J, \pi)}{2\pi}. \quad (4)$$

By then combining Eqs. (3) and (4), we obtain

$$f^{XL}(E_x, E_\gamma, J, \pi) = \frac{\mathcal{T}^{XL}(E_x, E_\gamma, J, \pi)}{2\pi E_\gamma^{2L+1}}. \quad (5)$$

By applying the generalized Brink-Axel hypothesis [24,25], the dependencies on E_x , J , and π are averaged out; i.e., the experimental γ -transmission coefficient represents an average transmission coefficient for all the spins accessible in the experiment, as well as for the excitation-energy range used in the extraction procedure. At high excitation energies, the γ transitions are dominantly of the dipole type ($L = 1$, see, e.g., Ref. [37]), and our experimental γ -transmission coefficient can be approximated by

$$\mathcal{T}(E_\gamma) \approx \mathcal{T}^{E1}(E_\gamma) + \mathcal{T}^{M1}(E_\gamma), \quad (6)$$

and thus we obtain the simplified expression

$$f(E_\gamma) = \frac{\mathcal{T}(E_\gamma)}{2\pi E_\gamma^3}, \quad (7)$$

where $f(E_\gamma)$ and $\mathcal{T}(E_\gamma)$ now represent the average total dipole GSF and γ -transmission coefficient, respectively. Using a χ^2 -minimization technique [30], it is possible to extract simultaneously the NLD and GSF from the quasicontinuum region in the first-generation matrix. For ^{166}Ho , the region between $E_x^{\min} = 1200$ keV, $E_x^{\max} = 6000$ keV, and $E_\gamma^{\min} = 1350$ keV was selected. This minimization technique is able to determine the functional, un-normalized form of the NLD and the GSF,

$$\tilde{\rho}(E_x - E_\gamma) = A e^{\alpha(E_x - E_\gamma)} \rho(E_x - E_\gamma), \quad (8a)$$

$$\tilde{\mathcal{T}}(E_\gamma) = B e^{\alpha E_\gamma} \mathcal{T}(E_\gamma), \quad (8b)$$

meaning that any value combination for the parameters A , B , and α would give a NLD and GSF pair compatible with the experimental results [30]. In order to fix the values of these three parameters, we have to normalize the two physical quantities by using known experimental data.

III. NORMALIZATION AND UNCERTAINTY PROPAGATION

A. Level density

The unnormalized NLD has two free parameters, A and α , so we need at least two external data points in order for these to be determined. Experimental values for the low

excitation-energy region in ^{166}Ho can be obtained by using the known discrete excitation-energy levels from Ref. [38]. In our case we observe a good fit for the region between $E_x = 0.26$ and 0.74 MeV, which we use for our normalization. At high excitation energies, we can calculate the total NLD value at the neutron separation energy S_n by using the measured level spacing D_0 of s -wave neutron resonances from, e.g., *Atlas of Neutron Resonances* [39]. We calculate the total NLD at S_n by [30]

$$\rho(S_n) = \frac{2\sigma_I^2}{D_0[(I_t + 1)e^{-(I_t+1)^2/2\sigma_I^2} + I_t e^{-I_t^2/2\sigma_I^2}]}, \quad (9)$$

where I_t is the spin of the target nucleus and σ_I is the spin cutoff parameter. The σ_I parameter must be estimated, which means we must assume a model for the spin distribution. Some well-known models include using the rigid-body moment of inertia (RMI) [40,41]

$$\sigma_I^2 = 0.0146A^{5/3}T \quad (10)$$

and the Fermi gas (FG) model from Gilbert and Cameron [42],

$$\sigma_I^2 = 0.0888A^{2/3}aT, \quad (11)$$

where A here is the nucleon number, a is the level density parameter, and T represents the nuclear temperature. The T parameter can be expressed by either the Gilbert and Cameron approach (CFG) [42],

$$T = \sqrt{U/a}, \quad (12)$$

or the formalism developed by von Egidy and Bucurescu (AFG) [40,41],

$$T = \frac{1 + \sqrt{1 + 4aU}}{2a}, \quad (13)$$

where in both cases $U = E_x - E_1$, where E_1 is a shift parameter. The parameters a and E_1 for ^{166}Ho are calculated using the prescription of Refs. [40,41]: $a = 18.277$ MeV $^{-1}$ and $E_1 = -0.949$ MeV for both models of the T parameter. As we have no reason to prefer one model above the other, we allow σ_I^2 to vary between 5.55 and 6.93. These values are listed in Table I. The chosen σ_I^2 uncertainty limits are reasonable when compared to the results of Uhrenholt *et al.* [23], where a study on ^{162}Dy shows that the ratio between the spin cutoff parameter at S_n from their combinatorial method and

Model	σ_I^2	$\rho(S_n)$ ($\times 10^6$ MeV $^{-1}$)
RMI + AFG	6.93	3.28
FG + CFG	5.55	2.32

the one calculated using the RMI model is 0.9, compared to 0.8 and 1.0 corresponding to the lower and upper limits we have chosen for ^{166}Ho .

Since any value between the two limits for σ_I^2 is, in principle, equally possible, we assume that the $\rho(S_n)$ error is flatly distributed between the values obtained by using the two σ_I^2 values in Eq. (9), as shown in Table I. The edges of the flat distribution are then smoothed with a Gaussian with a standard deviation calculated by propagating the uncertainties in the D_0 parameter. We obtain thus a flatly distributed $\rho(S_n)$ between 2.32×10^6 and $3.28 \times 10^6 \text{ MeV}^{-1}$, with a lower error of $0.08 \times 10^6 \text{ MeV}^{-1}$ and an upper error of $0.12 \times 10^6 \text{ MeV}^{-1}$.

Further, we need to extrapolate the experimental $\rho(E_x)$ data to S_n . In order to do this, we have considered two models. The first one is the constant-temperature (CT) model [42,43]:

$$\rho_{\text{CT}}(E_x) = \frac{1}{T_{\text{CT}}} \exp\left(\frac{E_x - E_0}{T_{\text{CT}}}\right), \quad (14)$$

where E_0 and T_{CT} are parameters representing the energy shift and the nuclear temperature, respectively. The second is the back-shifted Fermi gas (BSFG) model [42,44]:

$$\rho_{\text{BSFG}}(E_x) = \frac{\exp(2\sqrt{aU})}{12\sqrt{2}a^{1/4}U^{5/4}\sigma_I}, \quad (15)$$

where σ_I is the spin cutoff parameter, a is the level-density parameter, and $U = E_x - E_1$, where E_1 is the back-shift parameter. For convenience, we introduce an additional scaling parameter η in order to make the model reproduce the experimentally derived $\rho(S_n)$. For the best fit, η was found to be 0.507. While the NLD normalization parameters A and α are determined through the normalization procedure, the choice between the CT or the BSFG model comes down to the functional form of the experimental NLD data. While the CT model has a simple, exponential shape, the BSFG model is somewhat more curved due to the $\sim\sqrt{E_x}$ dependence. In order to decide which NLD model describes the experimental data best, we use an approach similar to that used in Guttormsen *et al.* [45] for ^{164}Dy . Here we run a χ^2 test for each model, where the model parameters are allowed to vary in order to minimize the χ^2 score. While the parameter values and the magnitudes of the χ^2 scores depend on the choice of A and α , the relationship between the χ^2 scores for the two models should not change, as this only depends on the functional shape of the NLD. The test gives a better χ^2 for the BSFG model by a factor of 1.5; therefore, this model is chosen for the extrapolation in the normalization procedure. Using a technique similar to the one presented in Ref. [46], we can propagate the normalization uncertainties to the whole NLD. By generating different NLDs with different combinations of the A and α parameters, we evaluate their goodness-of-fit to the selected region at low excitation energy and the calculated $\rho(S_n)$ by estimating a χ^2 score. For each E_x bin, we have many different $\rho(E_x)$ values, each with an associated χ^2 score. By plotting the χ^2 scores against $\rho(E_x)$ for each E_x bin, we can observe a parabolalike shape, from which we can graphically estimate the mean value of $\rho(E_x)$ to be the one for which $\chi^2 = \chi_{\text{min}}^2$, and the associated uncertainty where the $\chi^2 = \chi_{\text{min}}^2 + 1$ line crosses the parabola

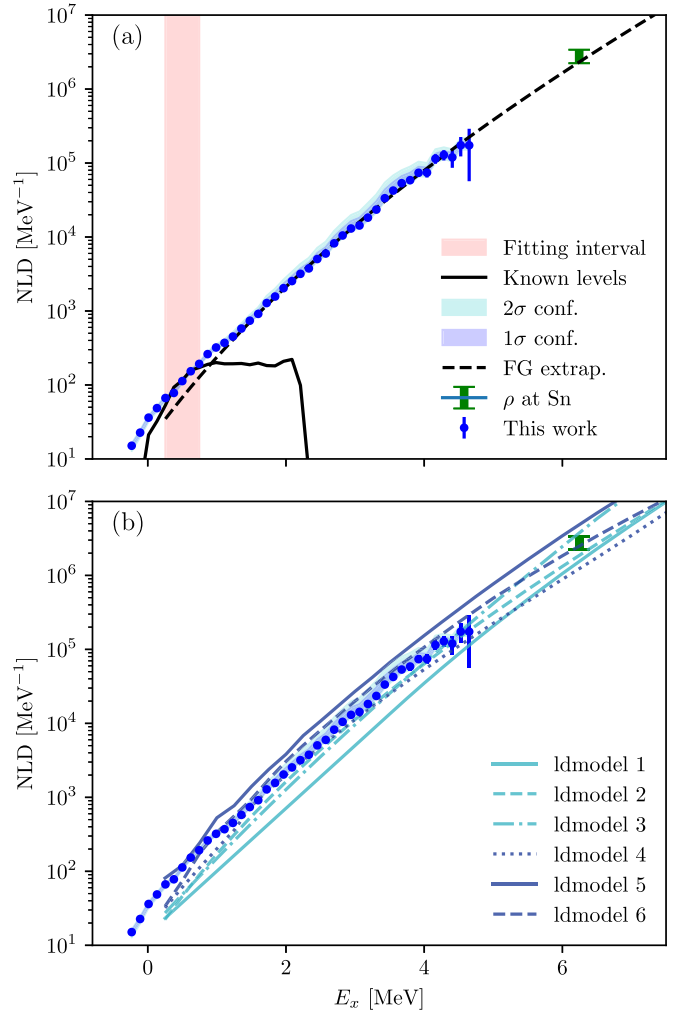


FIG. 2. The normalized NLD data points (see text). The uncertainties in the data points show the statistical and systematic uncertainties from the Oslo method analysis. In the total uncertainty band the systematic errors from the normalization are included. In panel (a), the normalized ^{166}Ho NLD is shown together with the fitting interval, the known levels, and the Fermi gas extrapolation to $\rho(S_n)$, while in panel (b) the same NLD is compared to the theoretical models from TALYS 1.95 [47,48]. The values are given as number of energy levels per MeV bin, where, e.g., the value at $E_x = 2 \text{ MeV}$ indicates the number of energy levels in the 1-MeV E_x interval between 1.5 and 2.5 MeV. This means that nonzero values for the NLD are expected down to $E_x = -0.5 \text{ MeV}$, the last one including the ground-state level at $E_x = 0 \text{ MeV}$.

(see Ref. [46] for details). The normalized NLD is shown in Fig. 2.

B. Gamma strength function

For the GSF, the parameter B in Eq. (8b) is found by normalizing it to the average total radiative width $\langle\Gamma_\gamma\rangle$ [32,49]. Experimental values for this quantity are available in Ref. [39], where for ^{166}Ho we find $84 \pm 5 \text{ meV}$. The average total radiative width of s -wave neutron capture resonances with spins $I_l \pm 1/2$ expressed in terms of the

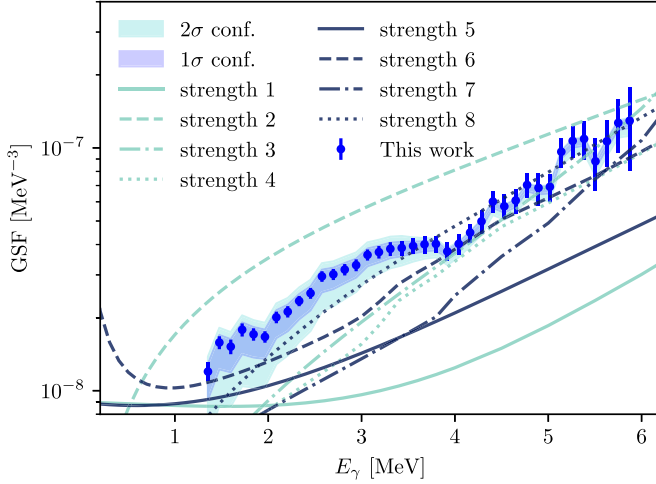


FIG. 3. The normalized GSF data points (see text). Here we include a comparison to the theoretical models (strength 1 to strength 8) used in TALYS 1.95 [47,48]. Uncertainties are displayed as in Fig. 2.

experimental \mathcal{T} is given by

$$\begin{aligned} & \langle \Gamma_\gamma(S_n, I_t \pm 1/2, \pi_t) \rangle \\ &= \frac{B}{4\pi \rho(S_n, I_t \pm 1/2, \pi_t)} \int_{E_\gamma=0}^{S_n} dE_\gamma \mathcal{T}(E_\gamma) \rho(S_n - E_\gamma) \\ & \times \sum_{J=-1}^1 g(S_n - E_\gamma, I_t \pm 1/2 + J), \end{aligned} \quad (16)$$

where I_t and π_t are the spin and parity of the target nucleus in the (n, γ) reaction, and $\rho(S_n - E_\gamma)$ is the experimental level density. Here it is assumed that there are equally many accessible levels with positive and negative parity for any excitation energy and spin, and again that dipole radiation is the dominant decay mechanism. Note that the factor $1/\rho(S_n, I_t \pm 1/2, \pi_t)$ equals the neutron resonance spacing D_0 . By assuming the uncertainty in $\langle \Gamma_\gamma \rangle$ to be normally distributed such that the given number represents one standard deviation from the mean, we can again use the same procedure as for the NLD used in Ref. [46] to propagate these uncertainties to the GSF. The results are shown in Fig. 3.

IV. RESULTS AND DISCUSSION

As anticipated from the NLD normalization discussed in Sec. III, the experimental ^{166}Ho NLD was found to be better described by the BSFG model than by the CT model. In Fig. 2 we present the normalized experimental NLD data together with the six theoretical models provided in TALYS 1.95 [47,48], where *ldmodel* 1, *ldmodel* 2, and *ldmodel* 3 are phenomenological models, and *ldmodel* 4, *ldmodel* 5, and *ldmodel* 6 are microscopical. For the three microscopical models the default values for c and δ were used, these being the two parameters for which the models can be adjusted to data. Although none of the models fits perfectly, we observe that the experimental data fall somewhat in the middle of the different suggested models. Overall, our data

points behave rather smoothly, as can be expected for an odd-odd nucleus with many available levels. In general, the GSF shows various features with different electromagnetic characters. Most notably for the energy region of this work ($E_\gamma \approx 1$ to 6 MeV), we expect the tail of the giant electric dipole resonance (GEDR, [50,51]), possibly the pygmy dipole resonance (PDR), (both of $E1$ character [52,53]), the spin-flip resonance, and the SR (both of $M1$ character [8]) to be present. As the Oslo method does not separate between $E1$ and $M1$ transitions, the GSF must be decomposed using models and/or auxiliary data. Figure 3 shows the GSF plotted together with the different theoretical models available in TALYS. Our data points are not well reproduced by any of the TALYS models, although an agreement when it comes to magnitude can be observed with the microscopic Gogny-HBF+QRPA model strength 8 [54]. Most of the models fail in predicting enough strength to match the experimental results, and none of them are able to describe properly the broad bump centered around $E_\gamma \approx 3$ MeV. The GSF in the $E_\gamma < S_n$ region is expected to be dominated by the tails of the GEDR and the PDR, as observed in the neighboring dysprosium isotopes [6]. Another interesting feature is the broad, resonancelike structure centered around $E_\gamma \approx 3$ MeV, which is a good candidate for the $M1$ scissors mode. This is the first observation of the mode in an odd-odd rare-earth nucleus with the Oslo method. In order to quantify the observed structures, the experimental GSF was decomposed into its constituent features. As for Dy isotopes and other deformed, rare-earth nuclei, we expect the GEDR of ^{166}Ho to be double-peaked [50,51]. Experimental GSF data for $E_\gamma > S_n$ for ^{166}Ho are not available, so data on ^{165}Ho have been used. There are data in the literature for this energy region from Berman *et al.* [55] and Bergère *et al.* [56], but their measured cross sections differ considerably. In order to resolve this conflict, a reanalysis of the two experiments has been carried out by Varlamov *et al.* [57], and the data from this re-evaluation have been used to model the $E1$ strength due to the GEDR. In order to fit the GEDR, a generalized Lorentzian (GLO) [37] is used:

$$f^{\text{GLO}}(E_\gamma) = \frac{\sigma_0 \Gamma_0}{3\pi^2 \hbar^2 c^2} \left(\frac{E_\gamma \Gamma_K}{(E_\gamma^2 - E_0^2)^2 + E_\gamma^2 \Gamma_K^2} + 0.7 \frac{\Gamma_{K,0}}{E_\gamma^3} \right), \quad (17)$$

where

$$\Gamma_K(E_\gamma, T_f) = \frac{\Gamma_0}{E_0^2} (E_\gamma^2 + 4\pi^2 T_f^2) \quad (18)$$

and $\Gamma_{K,0} = \Gamma_K(0, T_f)$. E_0 , Γ_0 , σ_0 , and T_f are fit parameters representing the energy centroid, the width, the peak cross section, and the temperature of the final levels, respectively. The PDR and the scissors mode are fitted using a standard Lorentzian (SLO),

$$f^{\text{SLO}}(E_\gamma) = \frac{1}{3\pi^2 \hbar^2 c^2} \frac{\sigma_s \Gamma_s^2 E_\gamma}{(E_\gamma^2 - E_s^2)^2 + E_\gamma^2 \Gamma_s^2}, \quad (19)$$

where E_s , Γ_s , and σ_s are again free parameters corresponding to the same quantities as for Eq. (17). In some other studies of the rare-earth region (see, e.g., Ref. [6]), a second $E1$ PDR was included in the fit, as well as the spin-flip $M1$ resonance.

The GLO already gives us a good fit of the GEDR without having to include these two structures, whose contribution is only noticeable in the $E_\gamma \approx 10$ MeV energy region, well beyond the range of this experiment. Our choice of fit functions reduces considerably the number of free parameters used in the fit.

Another interesting quantity to calculate is the experimental, integrated upward SR strength B_{SR} , defined as

$$B_{\text{SR}} = \frac{(3\hbar c)^3}{16\pi} \int f_{\text{SR}}(E_\gamma) dE_\gamma, \quad (20)$$

where f_{SR} is expressed by the fitted SLO in Eq. (19) to the broad structure at $E_\gamma \approx 3$ MeV. The result of the integration depends on the chosen limits, which should vary according to which work or experimental technique the result is to be compared with. Many NRF experiments have limited E_γ range and thus a smaller summed B_{SR} . When it comes to Oslo-method-like analyses, the decomposition of the GSF into two GEDR peaks (henceforth GEDR1 and GEDR2), a PDR and an SR, involves a series of challenges not only due to the high number of parameters involved but also because of the fact that OCL data cannot directly distinguish between $E1$ and $M1$ radiation. This is a particular problem for the SR, as its fit result is sensitive to the fitting parameters of the underlying $E1$ strength. In this work we show how we can attempt to solve these problems using three different methods. This provides us with a comparison of the different methods, as well as a tool in order to evaluate the uncertainties for the resulting B_{SR} . The first method (the “simultaneous fit”) is to fit all of the structures (the two peaks of the GEDR, the PDR and the SR) simultaneously. This gives the least χ^2 score, but also potentially underestimates the $E1$ strength yielding a potentially too big B_{SR} . The second method (the “two-step fit”) involves a fit of the GEDR first and a subsequent fit of the PDR and the SR by holding the newly found GEDR parameters fixed. This gives a higher χ^2 score, but a B_{SR} closer to previously determined values in this mass region. One of the most sensible parameters in the fit is the temperature T_0 . In both methods, the fit was run by holding the temperature fixed to either $T = 0.59$ MeV or $T = 0.66$ MeV, these corresponding to the calculated values from von Egidy and Bucurescu [40] for the CT and BSFG models, respectively. The resulting parameters from the first two fitting methods are shown in Table II, where method 1 corresponds to the simultaneous fit, method 2 corresponds to the two-steps fit, and (A) and (B) both indicate whether the CT value or the BSFG value for the temperature parameter was used. Figure 4 shows the obtained decomposition using method 2(A) as an example.

The third method (the “exponential background fit”), used among others by Nyhus *et al.* [4], Malatji *et al.* [60], and Agvaanluvsan *et al.* [19] involves approximating the $E1$ strength “background” as an exponential function of the form Ae^{cE_γ} , where A and c are parameters to be tuned to make the function go through the two points estimated to be the end points of the SR. When the background is subtracted, the excess strength can be integrated numerically to find B_{SR} (see Fig. 5). This last method does not involve a fit to the SR and thus gives no E_s , Γ_s , and σ_s parameters to compare to other works, but it

TABLE II. The parameters for the functions fitting the ^{166}Ho GSF (see text) Method 1 refers to the “simultaneous fit,” while Method 2 refers to the “two-step fit.” The labels (A) and (B) refer to the different choices in temperature.

Method	Function	T_0 (MeV)	$E_{0,s}$ (MeV)	$\Gamma_{0,s}$ (MeV)	$\sigma_{0,s}$ (mb)
1(A)	GEDR1	0.59	12.359(1)	3.35(3)	324(1)
	GEDR2	0.59	14.78(1)	1.89(3)	189(2)
	PDR		5.92(8)	1.96(12)	4.4(3)
	SR		3.14(7)	0.98(9)	0.43(3)
1(B)	GEDR1	0.66	12.341(1)	3.22(3)	330(1)
	GEDR2	0.66	14.78(1)	1.89(3)	195(2)
	PDR		5.58(40)	1.40(10)	3.8(3)
	SR		3.18(7)	0.80(4)	0.44(3)
2(A)	GEDR1	0.59	12.40(12)	3.50(4)	323(3)
	GEDR2	0.59	14.80(15)	1.82(2)	183(2)
	PDR		6.07(11)	1.89(3)	5.0(2)
	SR		3.20(12)	1.00(30)	0.40(8)
2(B)	GEDR1	0.66	12.38(12)	3.37(3)	330(3)
	GEDR2	0.66	14.79(15)	1.82(2)	188(2)
	PDR		5.48(17)	1.06(2)	4.1(9)
	SR		3.29(12)	0.98(26)	0.43(8)

gives perhaps the most reasonable estimate for the lowest limit of B_{SR} . An argument in support of this third approach is that the $E1$ modeling is not dependent on the description of the GEDR peaks and the PDR, and also because an SLO fit may not always be the best tool to describe a structure that is often fragmented and not necessarily resonance-shaped. However, the resulting integrated SR strength is indeed dependent on the choice of the two points enclosing the SR structure used

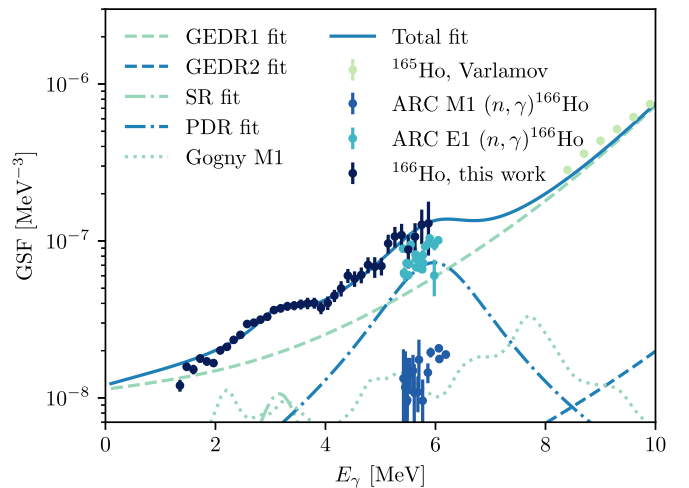


FIG. 4. Decomposition of the GSF into its underlying structures, using method 2(A), where the ^{165}Ho data for $E_\gamma > 6$ MeV from Varlamov *et al.* [57] were used to fit the double-peaked GEDR. The dotted line is the theoretical prediction from the deformed-basis QRPA calculations for $M1$ excitations on the ground state [58] and is compared to the average resonance capture (ARC) data from Ref. [59] for both $E1$ and $M1$ transitions.

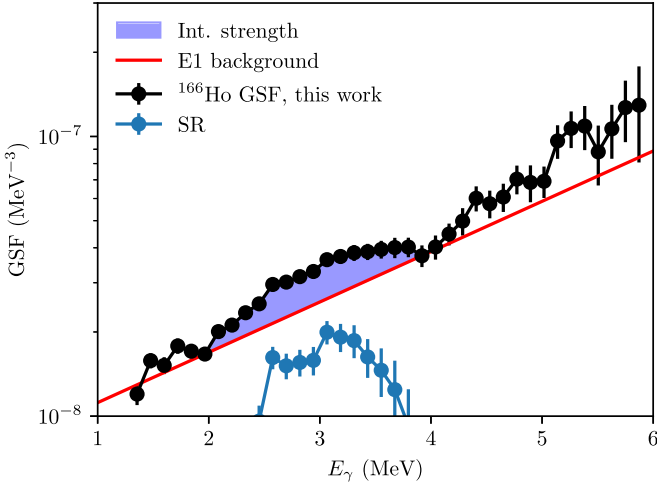


FIG. 5. The SR integrated strength evaluated by selecting the energy range of the SR and modeling the $E1$ background as an exponential going through the two outermost GSF points (see text). Shown in black are the data from the present work, in red (dark gray) the modeled $E1$ background as an exponential, and in blue (lighter gray) the residual strength obtained by subtracting the $E1$ component from the GSF data. This plot corresponds to the $E1$ fitting for method 3(B).

to fit the exponential background. Although the choice for the upper limit might fall naturally in the “kink” of the GSF at about $E_\gamma \approx 4$ MeV, the lower limit is more difficult to determine unambiguously. In order to reflect this uncertainty, we have calculated B_{SR} using two different exponential “background” fits, one choosing the first fitting point to be at $E_\gamma = 1.6$ MeV and the other at $E_\gamma = 2.0$ MeV. We denote these two variants of the third method as method 3(A) and method 3(B), respectively.

In Table III the fitting parameters for the different fits of the SR are shown, together with the calculated summed strengths B_{SR} for both the integration range $E_\gamma = 2.0$ – 4.0 MeV (comparable to the one used in NRF experiments) and the integration range $E_\gamma = 0.0$ – 10.0 MeV (for a more complete B_{SR} integration).

These results can be compared to those for neighboring isotopes. As many other nuclei have been analyzed using the Oslo method, we have the possibility to systematically study the different centroids, widths, and peak cross sections of the SR fitted by SLOs for the rare-earth region. In Fig. 6 are collected the results for Nd [63], Sm [18,60–62,64], Dy [6],

TABLE III. The integrated SR strengths for both the $E_\gamma = 2.0$ – 4.0 MeV range and the $E_\gamma = 0.0$ – 10.0 MeV range (see text).

Method	$B_{\text{SR}}^{2.0-4.0} (\mu_N^2)$	$B_{\text{SR}}^{0.0-10.0} (\mu_N^2)$
1(A)	3.3(4)	4.2(5)
1(B)	2.9(2)	3.5(3)
2(A)	3.1(15)	4.0(15)
2(B)	3.2(10)	4.1(14)
3(A)	2.9(5)	3.0(6)
3(B)	3.1(6)	3.2(6)

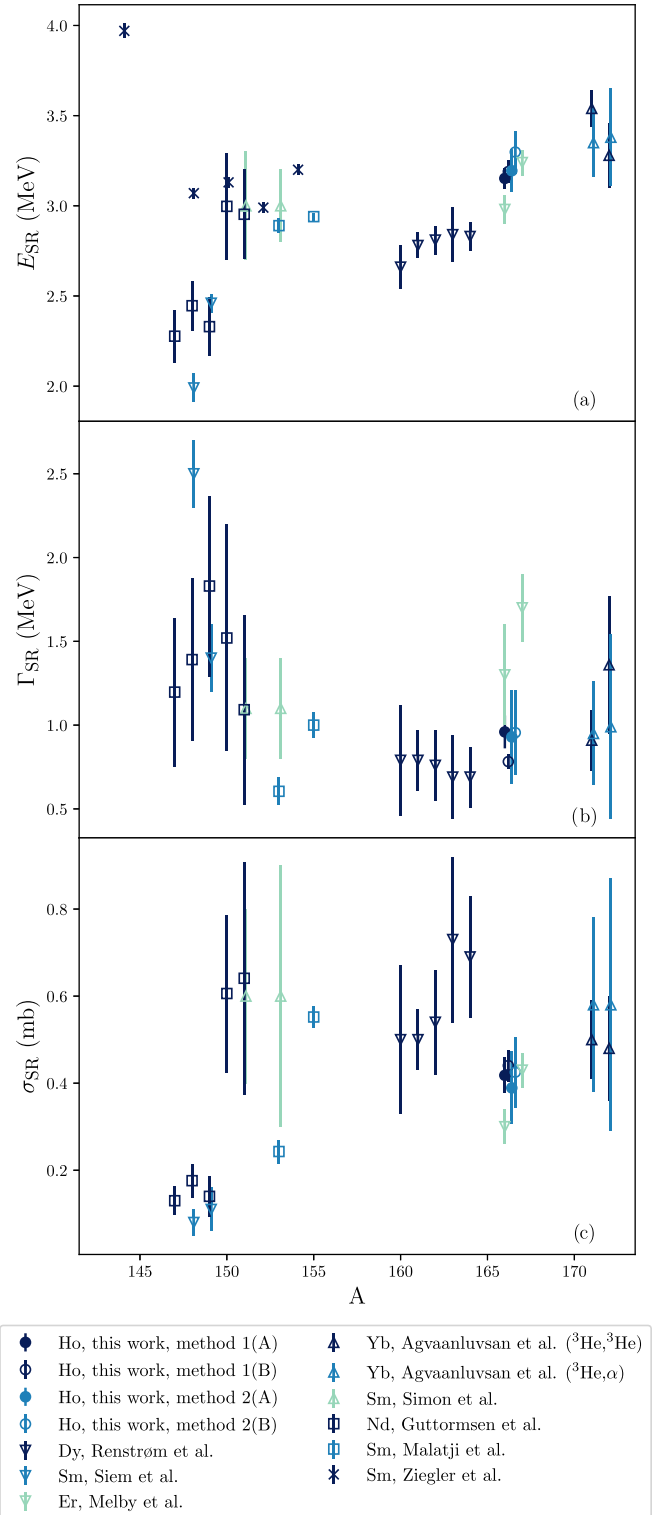


FIG. 6. Plot showing the values of the SLO fitting parameters for the SR collected for different deformed rare-earth nuclei (Refs. [6,17–19,60–64]), where panel (a) shows the centroids, panel (b) shows the widths, and panel (c) show the cross sections. Data obtained using the Oslo method are shown with triangles and squares, while a cross indicates another experiment modality (e.g., NRF). The results from the present work are shown with empty and solid circles.

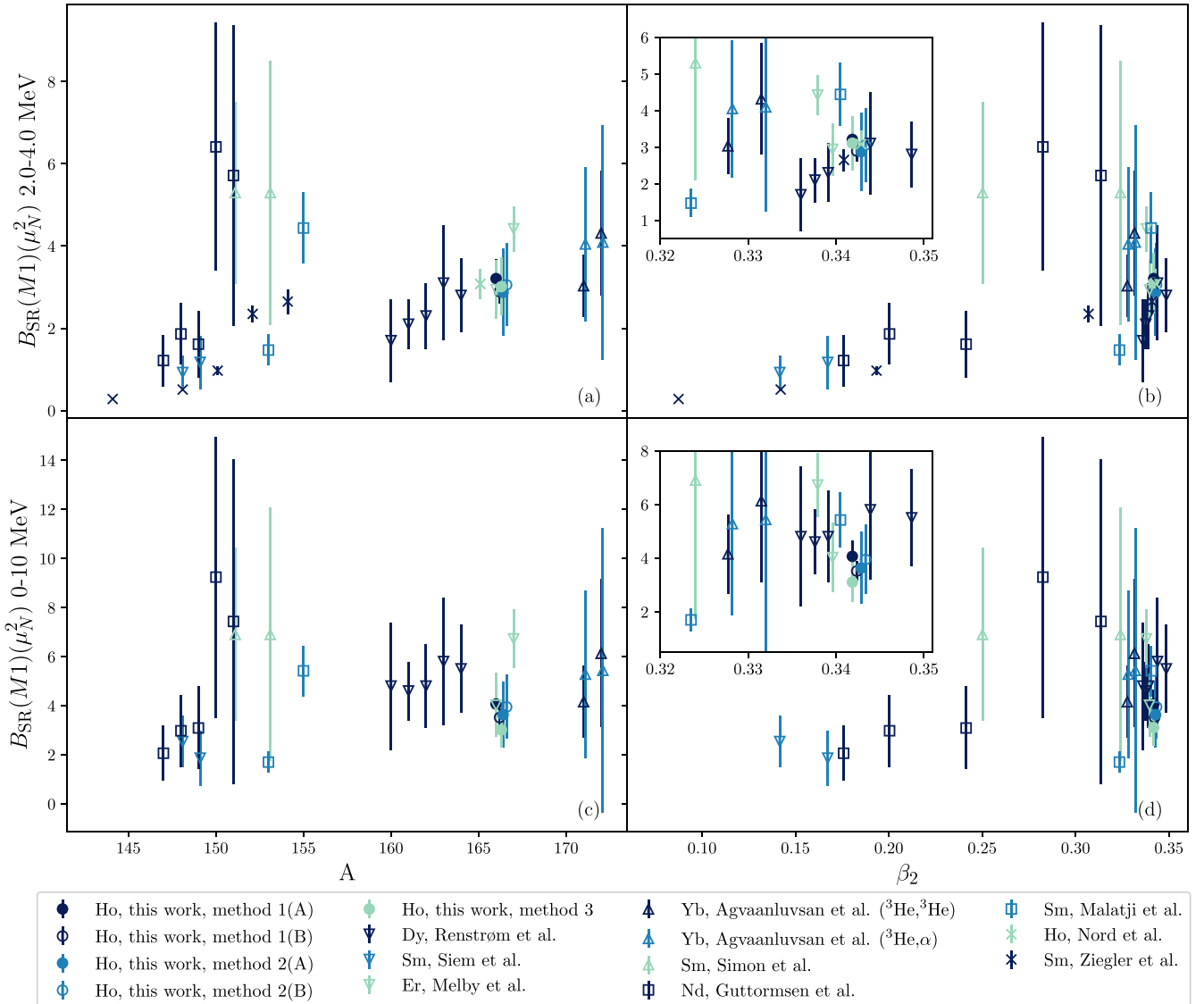


FIG. 7. In these graphs the SR strength B_{SR} collected from Refs. [6,13,17–19,60,62–64] is integrated between two regions: $E_\gamma = 2.0\text{--}4.0$ MeV in panels (a) and (b), and $E_\gamma = 0.0\text{--}10.0$ MeV in panels (c) and (d), and is plotted against the mass number in panels (a) and (c) and against the deformation parameter β_2 in panels (b) and (d) (region where $0.32 \leq \beta_2 \leq 0.35$ in the smaller inset plots). Circles, triangles, and squares indicate Oslo method data, and crosses indicate other experimental or analytical techniques (e.g., NRF). The data from Ziegler *et al.* [64] are integrated between 0 and 5 MeV.

Er [17], and Yb [19], where the results from Ziegler *et al.* [64] are results from a NRF experiment and only provide the energy centroid information. Together with these, the results for ^{160}Ho from the present work are included. There is no very clear pattern emerging from the plots in Fig. 6, as the results generally seem to be scattered. Nevertheless, in Fig. 6(a) we observe that the values for E_{SR} increase until $A \approx 150$, then remain constant, and finally increase again from about $E_{\text{SR}} \approx 2.7$ MeV for ^{160}Dy to $E_{\text{SR}} \approx 3.4$ MeV for ^{172}Yb . The results from this work fit nicely between those for dysprosium by Renstrøm *et al.* [6], erbium by Melby *et al.* [17], and ytterbium by Agvaanluvsan *et al.* [19]. This pattern does not correspond to what we would expect from the study by Enders *et al.* [12], which describes a constant or slowly decreasing value for E_{SR} between 3 and 3.5 MeV. Theoretical predictions for E_{SR} can

be obtained using the sum-rule approach [65], following the procedure in Ref. [12] replacing the ground-state moment of inertia with the rigid-body moment of inertia (following the same steps as in Guttormsen *et al.* [21]). From this approach a value of $E_{\text{SR}} = 2.89$ MeV is found by using $\beta_2 = 0.342$ as a value for the deformation, the average of those listed for ^{164}Dy and ^{168}Er in Ref. [66]. This is close but lower than the evaluated errors for all four values listed in Table II. Using the value from the FRDM evaluation by Möller *et al.* [67], $\beta_2 = 0.296$, we obtain an even lower value of $E_{\text{SR}} = 2.55$ MeV. The width Γ_{SR} and the peak cross section σ_{SR} are also plotted in Figs. 6(b) and 6(c), respectively. Here results are more scattered, although a possibly decreasing trend could be noticed for Γ_{SR} , and a possibly increasing one could be noticed for σ_{SR} .

In Fig. 7 are shown the SR strengths for two different integration intervals: $E_\gamma = 2.0\text{--}4.0$ MeV and $E_\gamma = 0.0\text{--}10.0$ MeV calculated by means of Eq. (20). These are in turn plotted against the mass number A and the deformation parameter β_2 retrieved from the evaluations in the *Atomic Data and Nuclear Data Tables* of Ref. [66]. The data for odd nuclei were obtained by averaging between neighboring even-even nuclei. These values were preferred to the FRDM evaluation by Möller *et al.* [67] as the latter tends to systematically undervalue the values calculated from $B(E2)$ experimental values. In Fig. 7 the calculated data from ^{166}Ho are plotted in five solid or empty circles, where the value for method 3 is the average of (A) and (B) (see Table III). Again we can compare to the plots in Enders *et al.* [12], where in Fig. 4 we notice how B_{SR} increases sharply at $A \approx 150$ from 1 to $3.5 \mu_N^2$, remains somewhat constant until $A \approx 170$ when it starts to slowly diminish. The data collected in Enders *et al.* [12] have a limited integration range (2.5 to 4.0 MeV), so it is best compared to Fig. 7(a). Although one might argue that the data may show an increase at around $A = 150$, these go all the way up to $6 \mu_N^2$ for Nd and Sm isotopes, and no flat or diminishing pattern is observed afterwards. Figure 7(c) shows the whole integrated SR strength, and again, although the pattern may seem similar to Fig. 4 in Enders *et al.* [12], the values are much larger. A different pattern appears when B_{SR} is plotted against deformation in Figs. 7(b) and 7(d). In both, and more clearly in Fig. 7(d), we notice how the strength increases gradually with deformation and reaches an apparent top at $\beta_2 \approx 0.28$, before decreasing. Many of the collected data sets agree in the value of B_{SR} at $\beta_2 \approx 0.34$. The experimental B_{SR} for ^{166}Ho can be again compared to the theoretical one obtained with the sum-rule approach, from which we obtain a value of $B_{\text{SR}} = 7.9 \mu_N^2$ using $\beta_2 = 0.342$ from Ref. [66], a value above the upper error limit for all methods. The same conclusion is

reached by using the possibly undervalued evaluated deformation $\beta_2 = 0.296$ from Ref. [67], where the value $B_{\text{SR}} = 6.9 \mu_N^2$ is obtained.

V. SUMMARY

In this work the data from the $^{163}\text{Dy}(\alpha, p\gamma)^{166}\text{Ho}$ experiment were analyzed using the Oslo method, and the NLD and GSF for ^{166}Ho were extracted. The resulting GSF presents typical features of a rare-earth, deformed, neutron-rich nucleus, such as a pygmy resonance at $E_\gamma \approx 6$ MeV and a peak compatible to the $M1$ scissors resonance at 3 MeV. This is the first time such a structure has been observed in an odd-odd nucleus with the Oslo method, confirming previous observations in ^{160}Tb where the two-step cascade method was used [9]. The SR strength has been extracted using three different methods, and while there is a spread in the measured values, they all yield results compatible to nuclei of similar mass number, and even more so to nuclei of similar deformation.

ACKNOWLEDGMENTS

We thank Pawel Sobas, Victor Modamio, and Jon C. Wikne at the Oslo Cyclotron Laboratory for operating the cyclotron and providing excellent experimental conditions and Erlend Lima, Gry Merete Tveten, and Fabio Zeiser for taking shifts during the experiment. A.C.L. gratefully acknowledges funding from the Research Council of Norway, Grant No. 316116, and from the European Research Council through ERC-STG-2014 under Grant No. 637686. V.W.I., A.G., and S.S. gratefully acknowledge financial support from the Research Council of Norway, Project No. 325714. E.F.M. and A.S.V. acknowledge support from the INTPART program from the Research Council of Norway, Project No. 310094.

-
- [1] J. P. Delaroche, M. Girod, J. Libert, H. Goutte, S. Hilaire, S. Péru, N. Pillet, and G. F. Bertsch, Structure of even-even nuclei using a mapped collective Hamiltonian and the DIS Gogny interaction, *Phys. Rev. C* **81**, 014303 (2010).
 - [2] M. Guttormsen, J. Rekestad, A. Henriquez, F. Ingebretsen, and T. F. Thorsteinsen, Nonstatistical Cooling of the Highly Excited ^{161}Dy Nucleus, *Phys. Rev. Lett.* **52**, 102 (1984).
 - [3] M. Guttormsen, A. Bagheri, R. Chankova, J. Rekestad, S. Siem, A. Schiller, and A. Voinov, Thermal properties and radiative strengths in $^{160,161,162}\text{Dy}$, *Phys. Rev. C* **68**, 064306 (2003).
 - [4] H. T. Nyhus, S. Siem, M. Guttormsen, A. C. Larsen, A. Bürger, N. U. H. Syed, G. M. Tveten, and A. Voinov, Radiative strength functions in $^{163,164}\text{Dy}$, *Phys. Rev. C* **81**, 024325 (2010).
 - [5] H. T. Nyhus, S. Siem, M. Guttormsen, A. C. Larsen, A. Bürger, N. U. H. Syed, H. K. Toft, G. M. Tveten, and A. Voinov, Level density and thermodynamic properties of dysprosium isotopes, *Phys. Rev. C* **85**, 014323 (2012).
 - [6] T. Renstrøm, H. Utsunomiya, H. T. Nyhus, A. C. Larsen, M. Guttormsen, G. M. Tveten, D. M. Filipescu, I. Gheorghie, S. Goriely, S. Hilaire, Y.-W. Lui, J. E. Midtbø, S. Péru, T. Shima, S. Siem, and O. Tesileanu, Verification of detailed balance for γ absorption and emission in Dy isotopes, *Phys. Rev. C* **98**, 054310 (2018).
 - [7] N. Lo Iudice and F. Palumbo, New Isovector Collective Modes in Deformed Nuclei, *Phys. Rev. Lett.* **41**, 1532 (1978).
 - [8] K. Heyde, P. von Neumann-Cosel, and A. Richter, Magnetic dipole excitations in nuclei: Elementary modes of nucleonic motion, *Rev. Mod. Phys.* **82**, 2365 (2010).
 - [9] J. Kroll, F. Bečvář, M. Krtička, and I. Tomandl, Photon strength functions of ^{160}Tb from the two-step gamma cascade measurement, *Int. J. Mod. Phys. E* **20**, 526 (2011).
 - [10] N. Huxel, P. von Brentano, J. Eberth, J. Enders, R.-D. Herzberg, P. von Neumann-Cosel, N. Nicolay, N. Pietralla, H. Prade, C. Rangacharyulu, J. Reif, A. Richter, C. Schlegel, R. Schwengner, S. Skoda, H. G. Thomas, I. Wiedenhöver, G. Winter, and A. Zilges, Complete scissors mode strength in heavy deformed odd-mass nuclei: a case study of ^{165}Ho and ^{169}Tm , *Nucl. Phys. A* **645**, 239 (1999).
 - [11] N. Pietralla, P. von Brentano, R.-D. Herzberg, U. Kneissl, N. Lo Iudice, H. Maser, H. H. Pitz, and A. Zilges, Systematics of the excitation energy of the 1^+ scissors mode and its empirical dependence on the nuclear deformation parameter, *Phys. Rev. C* **58**, 184 (1998).
 - [12] J. Enders, P. von Neumann-Cosel, C. Rangacharyulu, and A. Richter, Parameter-free description of orbital magnetic dipole strength, *Phys. Rev. C* **71**, 014306 (2005).

- [13] A. Nord, J. Enders, A. E. de Almeida Pinto, D. Belic, P. von Brentano, C. Fransen, U. Kneissl, C. Kohstall, A. Linnemann, P. von Neumann-Cosel, N. Pietralla, H. H. Pitz, A. Richter, F. Stedile, and V. Werner, Low-energy photon scattering experiments of $^{151,153}\text{Eu}$, ^{163}Dy , and ^{165}Ho and the systematics of the $M1$ scissors mode in odd-mass rare-earth nuclei, *Phys. Rev. C* **67**, 034307 (2003).
- [14] M. Krtička, F. Bečvář, J. Honzátko, I. Tomanđl, M. Heil, F. Käppeler, R. Reifarth, F. Voss, and K. Wisshak, Evidence for $M1$ Scissors Resonances Built on the Levels in the Quasicontinuum of ^{163}Dy , *Phys. Rev. Lett.* **92**, 172501 (2004).
- [15] A. Schiller, A. Voinov, E. Algin, J. Becker, L. Bernstein, P. Garrett, M. Guttormsen, R. Nelson, J. Reksad, and S. Siem, Low-energy $M1$ excitation mode in ^{172}Yb , *Phys. Lett. B* **633**, 225 (2006).
- [16] S. Valenta, B. Baramsai, T. A. Bredeweg, A. Couture, A. Chyżh, M. Jandel, J. Kroll, M. Krtička, G. E. Mitchell, J. M. O'Donnell, G. Rusev, J. L. Ullmann, and C. L. Walker, Examination of photon strength functions for $^{162,164}\text{Dy}$ from radiative capture of resonance neutrons, *Phys. Rev. C* **96**, 054315 (2017).
- [17] E. Melby, M. Guttormsen, J. Reksad, A. Schiller, S. Siem, and A. Voinov, Thermal and electromagnetic properties of ^{166}Er and ^{167}Er , *Phys. Rev. C* **63**, 044309 (2001).
- [18] S. Siem, M. Guttormsen, K. Ingeberg, E. Melby, J. Reksad, A. Schiller, and A. Voinov, Level densities and γ -strength functions in $^{148,149}\text{Sm}$, *Phys. Rev. C* **65**, 044318 (2002).
- [19] U. Agvaanluvsan, A. Schiller, J. A. Becker, L. A. Bernstein, P. E. Garrett, M. Guttormsen, G. E. Mitchell, J. Reksad, S. Siem, A. Voinov, and W. Younes, Level densities and γ -ray strength functions in $^{170,171,172}\text{Yb}$, *Phys. Rev. C* **70**, 054611 (2004).
- [20] M. Guttormsen, L. A. Bernstein, A. Bürger, A. Görden, F. Gunsing, T. W. Hagen, A. C. Larsen, T. Renstrøm, S. Siem, M. Wiedeking, and J. N. Wilson, Observation of Large Scissors Resonance Strength in Actinides, *Phys. Rev. Lett.* **109**, 162503 (2012).
- [21] M. Guttormsen, L. A. Bernstein, A. Görden, B. Jurado, S. Siem, M. Aiche, Q. Ducasse, F. Giacoppo, F. Gunsing, T. W. Hagen, A. C. Larsen, M. Lebois, B. Leniau, T. Renstrøm, S. J. Rose, T. G. Tornyi, G. M. Tveten, M. Wiedeking, and J. N. Wilson, Scissors resonance in the quasicontinuum of Th, Pa, and U isotopes, *Phys. Rev. C* **89**, 014302 (2014).
- [22] T. G. Tornyi, M. Guttormsen, T. K. Eriksen, A. Görden, F. Giacoppo, T. W. Hagen, A. Krasznahorkay, A. C. Larsen, T. Renstrøm, S. J. Rose, S. Siem, and G. M. Tveten, Level density and γ -ray strength function in the odd-odd ^{238}Np nucleus, *Phys. Rev. C* **89**, 044323 (2014).
- [23] H. Uehnholt, S. Åberg, A. Dobrowolski, T. Døssing, T. Ichikawa, and P. Möller, Combinatorial nuclear level-density model, *Nucl. Phys. A* **913**, 127 (2013).
- [24] D. M. Brink, Doctoral thesis, some aspects of the interaction of fields with matter, Oxford University, 1955.
- [25] P. Axel, Electric dipole ground-state transition width strength function and 7-MeV photon interactions, *Phys. Rev.* **126**, 671 (1962).
- [26] F. Zeiser, G. M. Tveten, F. L. Bello Garrote, M. Guttormsen, A.-C. Larsen, V. W. Ingeberg, A. Görden, and S. Siem, The γ -ray energy response of the Oslo Scintillator Array OSCAR, *Nucl. Instrum. Methods Phys. Res., Sect. A* **985**, 164678 (2021).
- [27] M. Guttormsen, A. Bürger, T. E. Hansen, and N. Lietaer, *Nucl. Instrum. Methods Phys. Res., Sect. A* **648**, 168 (2011).
- [28] M. Guttormsen, T. Tveter, L. Bergholt, F. Ingebretsen, and J. Reksad, The unfolding of continuum γ -ray spectra, *Nucl. Instrum. Methods Phys. Res., Sect. A* **374**, 371 (1996).
- [29] M. Guttormsen, T. Ramsøy, and J. Reksad, The first generation of γ -rays from hot nuclei, *Nucl. Instrum. Methods Phys. Res., Sect. A* **255**, 518 (1987).
- [30] A. Schiller, L. Bergholt, M. Guttormsen, E. Melby, J. Reksad, and S. Siem, Extraction of level density and γ strength function from primary γ spectra, *Nucl. Instrum. Methods Phys. Res., Sect. A* **447**, 498 (2000).
- [31] F. Zeiser and G. M. Tveten, oslocyclotronlab/OCL_GEANT4: Geant4 model of OSCAR, 2020, <https://doi.org/10.5281/zenodo.4018494>.
- [32] A. C. Larsen, M. Guttormsen, M. Krtička, E. Běták, A. Bürger, A. Görden, H. T. Nyhus, J. Reksad, A. Schiller, S. Siem, H. K. Toft, G. M. Tveten, A. V. Voinov, and K. Wikan, Analysis of possible systematic errors in the Oslo method, *Phys. Rev. C* **83**, 034315 (2011).
- [33] P. A. M. Dirac, The quantum theory of the emission and absorption of radiation, *Proc. R. Soc. London, Ser. A* **114**, 243 (1927).
- [34] E. Fermi, *Nuclear Physics* (The University of Chicago Press, Chicago, US, 1950).
- [35] G. A. Bartholomew, E. D. Earle, A. J. Ferguson, J. W. Knowles, and M. A. Lone, Gamma-ray strength functions, in *Advances in Nuclear Physics*, edited by M. Baranger and E. Vogt (Springer US, Boston, MA, 1973), Vol. 7, pp. 229–324.
- [36] J. M. Blatt and V. F. Weisskopf, *Theoretical Nuclear Physics*, 1st ed. (Springer, New York, 1952), p. 389.
- [37] J. Kopecky and M. Uhl, Test of gamma-ray strength functions in nuclear reaction model calculations, *Phys. Rev. C* **41**, 1941 (1990).
- [38] National Nuclear Data Center, information extracted from the NuDat database.
- [39] S. F. Mughabghab, *Atlas of Neutron Resonances: Resonance Properties and Thermal Cross Sections Z=1–100* (Elsevier, Amsterdam, 2018), Vol. 2.
- [40] T. von Egidy and D. Bucurescu, Systematics of nuclear level density parameters, *Phys. Rev. C* **72**, 044311 (2005).
- [41] T. von Egidy and D. Bucurescu, Erratum: Systematics of nuclear level density parameters [Phys. Rev. C **72**, 044311 (2005)], *Phys. Rev. C* **73**, 049901(E) (2006).
- [42] A. Gilbert and A. G. W. Cameron, A composite nuclear-level density formula with shell corrections, *Can. J. Phys.* **43**, 1446 (1965).
- [43] T. Ericson, The statistical model and nuclear level densities, *Adv. Phys.* **9**, 425 (1960).
- [44] T. Von Egidy, H. Schmidt, and A. Behkami, Nuclear level densities and level spacing distributions: Part II, *Nucl. Phys. A* **481**, 189 (1988).
- [45] M. Guttormsen, M. Aiche, F. L. Bello Garrote, L. A. Bernstein, D. L. Bleuel, Y. Byun, Q. Ducasse, T. K. Eriksen, F. Giacoppo, A. Görden, F. Gunsing, T. W. Hagen, B. Jurado, M. Klintefjord, A. C. Larsen, L. Lebois, B. Leniau, H. T. Nyhus, T. Renstrøm, S. J. Rose *et al.*, Experimental level densities of atomic nuclei, *Eur. Phys. J. A* **51**, 170 (2015).
- [46] F. Pogliano, A. C. Larsen, F. L. Bello Garrote, M. M. Bjørøen, T. K. Eriksen, D. Gjestvang, A. Görden, M. Guttormsen, K. C. W. Li, M. Markova, E. F. Matthews, W. Paulsen, L. G. Pedersen, S. Siem, T. Storebakken, T. G. Tornyi, and J. E. Vevik, Indirect measurement of the $(n, \gamma)^{127}\text{Sb}$ cross section, *Phys. Rev. C* **106**, 015804 (2022).

- [47] A. König, S. Goriely, and S. Hilaire, TALYS-1.9, A nuclear reaction program, user manual, Technical Report, 2017.
- [48] A. König, D. Rochman, J.-C. Sublet, N. Dzysiuik, M. Fleming, and S. van der Marck, Tendl: Complete nuclear data library for innovative nuclear science and technology, *Nucl. Data Sheets* **155**, 1 (2019), Special Issue on Nuclear Reaction Data.
- [49] A. C. Larsen, M. Guttormsen, M. Krtička, E. Běták, A. Bürger, A. Görge, H. T. Nyhus, J. Rekstad, A. Schiller, S. Siem, H. K. Toft, G. M. Tveten, A. V. Voinov, and K. Wikan, Erratum: Analysis of possible systematic errors in the Oslo method [Phys. Rev. C **83**, 034315 (2011)], *Phys. Rev. C* **97**, 049901(E) (2018).
- [50] M. N. Harakeh and A. van der Woude, *Giant Resonances* (Oxford University, Oxford, 2001).
- [51] S. S. Dietrich and B. L. Berman, Atlas of photoneutron cross sections obtained with monoenergetic photons, *At. Data Nucl. Data Tables* **38**, 199 (1988).
- [52] D. Savran, T. Aumann, and A. Zilges, Experimental studies of the pygmy dipole resonance, *Prog. Part. Nucl. Phys.* **70**, 210 (2013).
- [53] A. Bracco, E. Lanza, and A. Tamii, Isoscalar and isovector dipole excitations: Nuclear properties from low-lying states and from the isovector giant dipole resonance, *Prog. Part. Nucl. Phys.* **106**, 360 (2019).
- [54] S. Goriely, S. Hilaire, S. Péru, and K. Sieja, Gogny-HFB+QRPA dipole strength function and its application to radiative nucleon capture cross section, *Phys. Rev. C* **98**, 014327 (2018).
- [55] B. L. Berman, M. A. Kelly, R. L. Bramblett, J. T. Caldwell, H. S. Davis, and S. C. Fultz, Giant resonance in deformed nuclei: Photoneutron cross sections for Eu^{153} , Gd^{160} , Ho^{165} , and W^{186} , *Phys. Rev.* **185**, 1576 (1969).
- [56] R. Bergère, H. Beil, and A. Veyssièrre, Photoneutron cross sections of La, Tb, Ho and Ta, *Nucl. Phys. A* **121**, 463 (1968).
- [57] V. V. Varlamov, A. I. Davydov, and V. D. Kaidarova, Evaluation of reliable cross sections of photoneutron reactions on ^{103}Rh and ^{165}Ho nuclei, *Phys. At. Nucl.* **82**, 212 (2019).
- [58] M. Martini, S. Péru, S. Hilaire, S. Goriely, and F. Lechaftois, Large-scale deformed quasiparticle random-phase approximation calculations of the γ -ray strength function using the Gogny force, *Phys. Rev. C* **94**, 014304 (2016).
- [59] S. Goriely, P. Dimitriou, M. Wiedeking, T. Belgya, R. Firestone, J. Kopecky, M. Krtička, V. Plujko, R. Schwengner, S. Siem, H. Utsunomiya, S. Hilaire, S. Péru, Y. S. Cho, D. M. Filipescu, N. Iwamoto, T. Kawano, V. Varlamov, and R. Xu, Reference database for photon strength functions, *Eur. Phys. J. A* **55**, 172 (2019).
- [60] K. L. Malatji, K. S. Beckmann, M. Wiedeking, S. Siem, S. Goriely, A. C. Larsen, K. O. Ay, F. L. Bello Garrote, L. C. Campo, A. Görge, M. Guttormsen, V. W. Ingeberg, P. Jones, B. V. Kheswa, P. von Neumann-Cosel, M. Ozgur, G. Potel, L. Pellegrini, T. Renstrøm, G. M. Tveten, and F. Zeiser, Statistical properties of the well deformed $^{153,155}\text{Sm}$ nuclei and the scissors resonance, *Phys. Rev. C* **103**, 014309 (2021).
- [61] K. Malatji (private communication).
- [62] A. Simon, M. Guttormsen, A. C. Larsen, C. W. Beausang, P. Humby, J. T. Harke, R. J. Casperson, R. O. Hughes, T. J. Ross, J. M. Allmond, R. Chyzh, M. Dag, J. Koglin, E. McCleskey, M. McCleskey, S. Ota, and A. Saastamoinen, First observation of low-energy γ -ray enhancement in the rare-earth region, *Phys. Rev. C* **93**, 034303 (2016).
- [63] M. Guttormsen, K. O. Ay, M. Ozgur, E. Algin, A. C. Larsen, F. L. Bello Garrote, H. C. Berg, L. Crespo Campo, T. Dahl-Jacobsen, F. W. Furmyr, D. Gjestvang, A. Görge, T. W. Hagen, V. W. Ingeberg, B. V. Kheswa, I. K. B. Kullmann, M. Klintefjord, M. Markova, J. E. Midtbø, V. Modamio *et al.*, Evolution of the γ -ray strength function in neodymium isotopes, *Phys. Rev. C* **106**, 034314 (2022).
- [64] W. Ziegler, C. Rangacharyulu, A. Richter, and C. Spieler, Orbital Magnetic Dipole Strength in $^{148,150,152,154}\text{Sm}$ and Nuclear Deformation, *Phys. Rev. Lett.* **65**, 2515 (1990).
- [65] E. Lipparini and S. Stringari, Sum rules and giant resonances in nuclei, *Phys. Rep.* **175**, 103 (1989).
- [66] B. Pritychenko, M. Birch, B. Singh, and M. Horoi, Tables of E2 transition probabilities from the first 2^+ states in even-even nuclei, *At. Data Nucl. Data Tables* **107**, 1 (2016).
- [67] P. Möller, A. Sierk, T. Ichikawa, and H. Sagawa, Nuclear ground-state masses and deformations: FRDM(2012), *At. Data Nucl. Data Tables* **109-110**, 1 (2016).